

Anisotropic Molecular Rotational Diffusion in ^{15}N Spin Relaxation Studies of Protein Mobility[†]

Peter Luginbühl, Konstantin V. Pervushin, Hideo Iwai, and Kurt Wüthrich*

Institut für Molekularbiologie und Biophysik, Eidgenössische Technische Hochschule-Hönggerberg, CH-8093 Zürich, Switzerland

Received December 27, 1996; Revised Manuscript Received March 27, 1997[⊗]

ABSTRACT: The backbone dynamics of the uniformly ^{15}N -labeled N-terminal 63-residue DNA-binding domain of the 434 repressor has been characterized by measurements of the individual ^{15}N longitudinal relaxation times, T_1 , transverse relaxation times, T_2 , and heteronuclear $^{15}\text{N}\{^1\text{H}\}$ -NOEs at ^1H resonance frequencies of 400 and 750 MHz. The dependence of an apparent spherical top correlation time, τ_R , on the orientation of the N–H bond vector with respect to the principal axes of the global diffusion tensor of the protein was used to establish the fact that the degree of anisotropy of the global molecular tumbling amounts to 1.2, which is in good agreement with the values obtained from model calculations of the hydrodynamic properties. A model-free analysis showed that even this small anisotropy leads to the implication of artifactual slow internal motions for at least two residues when the assumption of isotropic global motion is used. Additional residues may actually undergo internal motions on the same time scale as the global rotational diffusion, in which case the model-free approach would, however, be inappropriate for quantifying the correlation times and order parameters. Overall, the experiments with 434(1–63) demonstrate that the assumption of isotropic rotational reorientation may result in artifacts of model-free interpretations of spin relaxation data even for proteins with small deviations from spherical shape.

Nuclear spin relaxation measurements in solutions of uniformly ^{15}N -enriched proteins with the use of ^1H -detected two-dimensional (2D)¹ nuclear magnetic resonance (NMR) experiments are a popular approach for studies of global protein motions and internal backbone mobility (Barbato *et al.*, 1992; Broadhurst *et al.*, 1995; Clore *et al.*, 1990a; Farrow *et al.*, 1994a; Kay *et al.*, 1989; Lipari & Szabo, 1982a,b; Orekhov *et al.*, 1994, 1995a; Peng & Wagner, 1992; Peng *et al.*, 1991; Szyperski *et al.*, 1993; Tjandra *et al.*, 1995, 1996; Wagner, 1993). Thereby, measurements of the longitudinal and transverse relaxation times, $T_1(^{15}\text{N})$ and $T_2(^{15}\text{N})$, respectively, and the heteronuclear $^{15}\text{N}\{^1\text{H}\}$ -NOEs are subjected to combined analysis in terms of either a molecular model describing the random molecular motion (John & McClung, 1982; Kinoshita *et al.*, 1977; Lipari & Szabo, 1980; London & Avitabile, 1978; Richarz *et al.*, 1980; Tropp, 1980; Wallach, 1967; Wittebort & Szabo, 1978; Woessner, 1962a, 1965) or a model-free characterization of the system (Lipari & Szabo, 1982a,b). In the former approach, the parameters for the molecular motion are determined by a least-squares fit of the experimental relaxation data to those calculated from model-specific spectral density functions. With the model-free approach, one characterizes the system by values for the global rotational correlation time(s), effective internal correlation times, and generalized order parameters that define spatial restrictions of the internal motions. Although

in most ^{15}N relaxation studies of protein dynamics published so far the protein has been assumed to tumble isotropically, evidence questioning the general validity of this approximation has also been presented (Barbato *et al.*, 1992; Broadhurst *et al.*, 1995; Tjandra *et al.*, 1995, 1996). The present paper describes new results relating to this critical aspect of the analysis of spin relaxation data.

We selected the small globular protein 434(1–63), which corresponds to the N-terminal 63-residue DNA-binding domain of the 434 repressor, for this project. 434(1–63) can readily be expressed in large amounts in *Escherichia coli* and is soluble in water at high concentrations, which makes it a suitable system for performing high-precision relaxation measurements at different magnetic field strengths. For the analysis of the relaxation data, it is important that the molecular architecture of 434(1–63) in solution has been determined by NMR. It includes five α -helices with residues 2–13, 17–24, 28–35, 45–52, and 56–60 (Pervushin *et al.*, 1996) and is very similar to the corresponding segment of 434(1–69) both in crystals (Mondragon *et al.*, 1989) and in solution (Neri *et al.*, 1992). The second and third helices are connected by a tight turn, and the backbone conformation from residue 17 to 35 forms a classical helix–turn–helix motif (Brennan & Matthews, 1989). A first subdomain containing helices 1–3 and a second subdomain containing helices 4 and 5 are connected by a flexible loop of residues 36–44, which displays increased conformational disorder in the NMR solution structure (Pervushin *et al.*, 1996).

The global shape of 434(1–63) is nearly spherical so that we could investigate the influence of small anisotropy of the rotational diffusion on the ^{15}N relaxation parameters. Since the axes of the five helices adopt different angles with respect to the longest principal axis of inertia of the protein, and since the effects on the spectral density of anisotropy of

[†] Financial support was obtained from the Schweizerischer Nationalfonds (Project 31.32033.91).

[⊗] Abstract published in *Advance ACS Abstracts*, May 15, 1997.

¹ Abbreviations: NMR, nuclear magnetic resonance; 2D, two-dimensional; 434(1–63), N-terminal 63-residue DNA-binding domain of the 434 repressor; 434(1–69), N-terminal 69-residue DNA-binding domain of the 434 repressor; CPMG, Carr–Purcell–Meiboom–Gill; SMF, simple model-free approach; EMF, extended model-free approach; MMF, minimal model-free approach.

the overall motion depend on the orientation of the N–H bonds relative to the principal axes of the diffusion tensor, different relaxation behavior is expected for amide groups in different helices, whereas all amide groups within a given helix will relax at similar rates. Analysis of the mean properties of the five groups of helical residues was thus used to determine the degree of anisotropy of the rotational tumbling of the molecule, whereby $T_1(^{15}\text{N})$, $T_2(^{15}\text{N})$, and the heteronuclear $^{15}\text{N}\{^1\text{H}\}$ -NOE obtained for the individual residues were analyzed using the model-free approach (Lipari & Szabo, 1982a,b).

MATERIALS AND METHODS

Sample Preparation. 434(1–63) was cloned in *E. coli*, and the uniformly ^{15}N -labeled protein was expressed and purified as described previously (Neri *et al.*, 1992; G. Siegal, V. Dötsch, and K. Wüthrich, submitted for publication). The NMR sample used here contained 5 mM protein in 20 mM potassium phosphate buffer at pH 4.8 in a mixed solvent of 90% $\text{H}_2\text{O}/10\%$ D_2O .

NMR Spectroscopy. All experiments were performed at 13 °C, using Varian Unity-plus spectrometers operating at ^1H frequencies of 400 and 750 MHz. The pulse sequence used for measurements of $T_1(^{15}\text{N})$ has been adapted from Farrow *et al.* (1994b) by replacing the H^{N} -selective 180° proton pulse in the ^{15}N relaxation delay by a “hard” 180° pulse to minimize the influence of the ^1H radiofrequency carrier position on the suppression of the cross-correlation between dipolar relaxation and chemical shift anisotropy relaxation (Palmer *et al.*, 1992). The T_1 relaxation delays at 400 MHz were 11, 26, 76, 146, 196, 296, 396, 496, and 596 ms; at 750 MHz, they were 11, 86, 136, 196, 296, 396, 596, 896, 1196, and 1496 ms. Measurement of $T_2(^{15}\text{N})$ was based on a CPMG-type sequence (Farrow *et al.*, 1994a) so that effectively a spin-locked transverse relaxation time was measured (Peng *et al.*, 1991). The delay between the ^{15}N 180° pulses in the spin-lock train was 4 ms, which provided weakly spin-locked transverse ^{15}N magnetization. The use of weak spin-lock conditions ensured minimal suppression of line broadening contributions from chemical exchange to the measured $T_2(^{15}\text{N})$ values (Szyperski *et al.*, 1993). Since the $T_1(^{15}\text{N})$ and $T_2(^{15}\text{N})$ relaxation times were measured at 400 and 750 MHz for protons, the line broadening from chemical exchange could then be evaluated by the method of Orekhov *et al.* (1995a). The T_2 relaxation delays at 400 MHz were 10, 26, 50, 82, 98, 122, and 146 ms; at 750 MHz, they were 10, 26, 58, 90, 106, 138, and 170 ms. $^{15}\text{N}\{^1\text{H}\}$ -NOEs were measured using pulsed field gradients to suppress saturation-transfer artifacts which may arise from H_2O solvent preirradiation (Li & Montelione, 1994). All data sets were processed using the program PROSA (Güntert *et al.*, 1992), and peak picking and volume integration were performed with the program XEASY (Bartels *et al.*, 1995).

Relaxation Parameters and Spectral Densities. $T_1(^{15}\text{N})$, $T_2(^{15}\text{N})$, and the $^{15}\text{N}\{^1\text{H}\}$ -NOEs were related to spectral density functions, $J(\omega)$, by (Abragam, 1961)

$$\frac{1}{T_1} = \frac{3}{10} \left(\frac{\gamma_{\text{N}} \gamma_{\text{H}} \hbar}{r_{\text{NH}}^3} \right)^2 \left[\frac{1}{3} J(\omega_{\text{N}} - \omega_{\text{H}}) + J(\omega_{\text{N}}) + 2J(\omega_{\text{N}} + \omega_{\text{H}}) \right] + \frac{2}{15} (\omega_{\text{N}} \Delta\sigma_{\text{N}})^2 J(\omega_{\text{N}}) \quad (1)$$

$$\frac{1}{T_2} = \frac{3}{10} \left(\frac{\gamma_{\text{N}} \gamma_{\text{H}} \hbar}{r_{\text{NH}}^3} \right)^2 \left[\frac{2}{3} J(0) + \frac{1}{6} J(\omega_{\text{N}} - \omega_{\text{H}}) + \frac{1}{2} J(\omega_{\text{N}}) + J(\omega_{\text{H}}) + J(\omega_{\text{N}} + \omega_{\text{H}}) \right] + \frac{2}{15} (\omega_{\text{N}} \Delta\sigma_{\text{N}})^2 \left[\frac{2}{3} J(0) + \frac{1}{2} J(\omega_{\text{N}}) \right] \quad (2)$$

$$^{15}\text{N}\{^1\text{H}\}\text{-NOE} = \frac{\gamma_{\text{H}}}{\gamma_{\text{N}}} \frac{3}{10} \left(\frac{\gamma_{\text{N}} \gamma_{\text{H}} \hbar}{r_{\text{NH}}^3} \right)^2 \left[-\frac{1}{3} J(\omega_{\text{N}} - \omega_{\text{H}}) + 2J(\omega_{\text{N}} + \omega_{\text{H}}) \right] T_1 \quad (3)$$

where γ_i and ω_i are, respectively, the gyromagnetic ratio and the Larmor frequency of spin i and \hbar is Planck's constant divided by 2π . $\Delta\sigma_{\text{N}}$ is the difference between the axial and the perpendicular principal components of the axially symmetric ^{15}N chemical shift tensor, which is estimated to be -160 ppm for polypeptide backbone amide groups (Hiyama *et al.*, 1988). To account for contributions to T_2 from chemical or conformational exchange, an exchange term is added to eq 2,

$$\frac{1}{T_2(\text{obs})} = \frac{1}{T_2} + \pi\Delta_{\text{ex}} \quad (4)$$

where Δ_{ex} is the increase in line width due to exchange (McConnell, 1958; Allerhand *et al.*, 1965).

Models Used for the Data Analysis. For the analysis of global rotational motions, the simplest model is the rigid spherical top with the spectral density function (Abragam, 1961)

$$J(\omega) = \frac{\tau}{1 + (\omega\tau)^2}, \quad \tau^{-1} = 6D \quad (5)$$

where D is the rotational diffusion coefficient related to isotropic global Brownian motion.

A model that can account for asymmetry about two principal axes is the rigid symmetric top, for which the decay of the correlation function depends on the angle α between the N–H bond vector and the axis of symmetry. The resulting spectral density function has the form (Shimizu, 1962; Woessner, 1962b)

$$J(\omega) = \frac{1}{4} [3(\cos \alpha)^2 - 1]^2 \frac{\tau_{\text{A}}}{1 + (\omega\tau_{\text{A}})^2} + 3(\sin \alpha)^2 (\cos \alpha)^2 \frac{\tau_{\text{B}}}{1 + (\omega\tau_{\text{B}})^2} + \frac{3}{4} (\sin \alpha)^4 \frac{\tau_{\text{C}}}{1 + (\omega\tau_{\text{C}})^2} \quad (6)$$

where the individual correlation times depend on the rotational diffusion coefficients perpendicular and parallel to the axis of symmetry in the following manner:

$$\tau_{\text{A}}^{-1} = 6D_{\perp} \quad \tau_{\text{B}}^{-1} = 5D_{\perp} + D_{\parallel} \quad \tau_{\text{C}}^{-1} = 2D_{\perp} + 4D_{\parallel} \quad (7)$$

An average diffusion coefficient, D , can be defined with a corresponding average correlation time, τ :

$$D = \frac{1}{3} (D_{\parallel} + 2D_{\perp}); \quad \tau^{-1} = 6D = 2D_{\parallel} + 4D_{\perp} \quad (8)$$

In our treatment, the anisotropy for the symmetric top molecule model will be determined by fitting an apparent spherical top correlation time, τ_R , for each individual ^{15}N spin. The dependence of the individually measured τ_R values on the orientation of the N–H bond vector will then be used to provide information on the degree of anisotropy of the molecular tumbling. Thereby, the following qualitative relations are used as a general guideline. If the angle α between the N–H bond vector and the axis of symmetry is smaller than the magic angle of 54.7° , τ_R will be an overestimate of τ ; if α is larger than 54.7° , τ_R will be an underestimate of τ . If $\alpha = 54.7^\circ$, $\tau_R = \tau$. The ratio R of the longest correlation time, when $\alpha = 0^\circ$, and the shortest correlation time, when $\alpha = 90^\circ$, can be expressed in terms of the anisotropy of diffusion, $r = D_{\parallel}/D_{\perp}$, according to

$$R = \frac{(6D_{\perp})^{-1}}{\frac{1}{4}(6D_{\perp})^{-1} + \frac{3}{4}(2D_{\perp} + 4D_{\parallel})^{-1}} = \frac{4r + 2}{r + 5} \quad (9)$$

This can be rearranged to give

$$r = \frac{5R - 2}{4 - R} \quad (10)$$

Using simulated data, Schurr *et al.* (1994) demonstrated that the r value estimated from this equation exceeds the true anisotropy only slightly, by up to 8% when $r = 2.5$, when R is replaced by the ratio of the longest and the shortest best-fit τ_R values.

The model-free approach (Lipari & Szabo, 1982a,b) accounts for internal mobility through a correlation time for intramolecular motion, τ_s , and a corresponding generalized order parameter, S_s^2 . This treatment is applicable when the internal motion is rapid compared to the global rotational motion, *i.e.*, $\tau_s \ll \tau$. Commonly, the global rotational motion is assumed to be isotropic, which results in a spectral density of the functional form

$$J(\omega) = S_s^2 \frac{\tau}{1 + (\omega\tau)^2} + (1 - S_s^2) \frac{\tau_s'}{1 + (\omega\tau_s')^2} \quad (11)$$

with

$$\tau_s' = \frac{\tau\tau_s}{\tau + \tau_s} \quad (12)$$

The spectral density function of eq 11 will be referred to as the “simple model-free approach” (SMF). The generalized order parameter S_s^2 , which describes the amplitude of the internal motion, is equal to 1 if the internal motion is completely restricted and equal to 0 if the internal motion is isotropic. S_s^2 is derived from the NMR relaxation data in a model-free manner, but it can be interpreted within the framework of any given model to obtain a physical picture of the amplitude of the internal motions. For example, in the wobble-in-a-cone model (Lipari & Szabo, 1980; Richarz *et al.*, 1980), where the N–H bond vector diffuses freely in a cone of semiangle θ ,

$$S_s^2 = \left[\frac{1}{2} \cos \theta (1 + \cos \theta) \right]^2 \quad (13)$$

For relaxation data on backbone amide groups which cannot be accounted for by the two-parameter SMF, Clore *et al.* (1990b) proposed an approach based on the spectral density function

$$J(\omega) = S_f^2 S_s^2 \frac{\tau}{1 + (\omega\tau)^2} + (1 - S_f^2) \frac{\tau_f'}{1 + (\omega\tau_f')^2} + S_f^2 (1 - S_s^2) \frac{\tau_s'}{1 + (\omega\tau_s')^2} \quad (14)$$

with

$$\tau_f' = \frac{\tau\tau_f}{\tau + \tau_f}; \quad \tau_s' = \frac{\tau\tau_s}{\tau + \tau_s} \quad (15)$$

The subscripts f and s indicate faster and slower internal motions on significantly different time scales, respectively, and both must be rapid compared to the global rotational motion. Since the number of parameters usually exceeds the number of experimentally accessible data, it is commonly assumed that $\tau_f < 20$ ps. The second term in eq 14 is then negligibly small, which yields the “extended model-free approach” (EMF) with which the system studied is characterized by the parameters τ , S_f^2 , S_s^2 , and τ_s . If, in addition, the fast internal motion is completely restricted, *i.e.*, $S_f^2 = 1$, the EMF reduces to the SMF (eq 11), with the three parameters τ , S_s^2 , and τ_s . On the other hand, if the slow internal motion is completely restricted, *i.e.*, $S_s^2 = 1$, the EMF reduces to the “minimal model-free approach” (MMF), where the system is characterized by τ and a single parameter for the internal motion, S_f^2 .

Least-Squares Fit of Relaxation Parameters. The model-free analysis was performed using the program DASHA (Orekhov *et al.*, 1995b), where a model-free parameter set ζ is determined by nonlinear minimization of the penalty function χ^2 (Palmer *et al.*, 1991):

$$\chi^2(\zeta) = \sum_{i=1}^N \frac{[V_i^{\text{cal}}(\zeta) - V_i^{\text{exp}}]^2}{(\Delta V_i^{\text{exp}})^2} \quad (16)$$

where $V_i^{\text{cal}}(\zeta)$ and V_i^{exp} are the calculated and experimental relaxation parameters, respectively, ΔV_i^{exp} is the uncertainty of the experimental value, and the index i runs over all N available experimental data sets. Selection of the appropriate spectral density function was accomplished by initial fitting of the relaxation data to the simplest possible spectral density function and employing more complicated models only as required for improved fits of the experimental data. Thereby, a particular model-free formulation was considered to provide an adequate fit of the experimental data for a given residue when the value of χ^2 was smaller than 6.8 (Nicholson *et al.*, 1995). Estimates of the precision of the extracted model-free parameters were obtained by the Monte Carlo approach described by Kamath and Shriver (1989).

Hydrodynamic Calculations. The elements of the rotational diffusion tensor were estimated using the bead model description of one of the 20 energy-refined DIANA conformers that describe the NMR solution structure of 434-(1–63) at pH 4.8 (Pervushin *et al.*, 1996). In this approximation, a polymer is modeled as a collection of point sources of friction (beads) with hydrodynamic interactions described

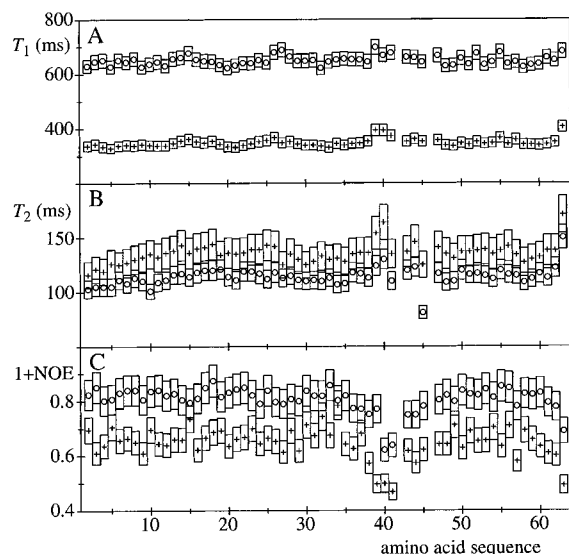


FIGURE 1: Plots of relaxation times $T_1(^{15}\text{N})$ and $T_2(^{15}\text{N})$ and the $^{15}\text{N}\{^1\text{H}\}$ -NOEs for 434(1–63) versus the amino acid sequence. Data measured at 400 MHz are represented by plus signs (+) and those at 750 MHz by circles (O). The vertical bars indicate the maximum errors in the measured data (see the text).

by the Oseen tensor (García de la Torre & Bloomfield, 1981). Diffusion coefficients were calculated for a temperature of 13 °C and an η of 1.202 cp (the viscosity of pure water at this temperature) using the modified Oseen tensor. The beads representing an amino acid residue were defined either as the C^α position, using a bead radius σ of 3.5 Å, or the positions of the backbone atoms N, C^α , and C' , with bead radii σ of 1.0 Å each (Barbato *et al.*, 1992). The module DIFFC of the program DASHA (Orekhov *et al.*, 1995b) was used for this part of the computations.

RESULTS

T_1 , T_2 , and NOE Data. The relaxation rates (Figure 1A,B) were determined by nonlinear least-squares fitting of the magnetization decay curves to a single-exponential function, using the Levenberg–Marquardt method (Press *et al.*, 1992). The average standard errors were, respectively, 2.0 and 1.5% for the T_1 data at 400 and 750 MHz and 4.1 and 2.9% for the corresponding T_2 data. The maximum errors in T_1 and T_2 were obtained by Monte Carlo-type procedures (Kamath & Shriver, 1989), which involved fitting of the intensity decay multiple times with random addition or subtraction of 5% of the measured peak volumes. The Monte Carlo-estimated errors are, respectively, 5.3 and 3.8% for the T_1 data at 400 and 750 MHz and 10.0 and 7.3% for the corresponding T_2 data and thus amount to approximately 2.5 times the corresponding average standard errors. The Monte Carlo-estimated errors for the $^{15}\text{N}\{^1\text{H}\}$ -NOEs at both 400 and 750 MHz are 6.7%.

Global Rotational Correlation Time Evaluated Using the Spherical Top Model. Assuming a spherical top molecule, we derived a single effective global correlation time, τ_c , for all residues simultaneously, as previously described by Kay *et al.* (1989) and Clore *et al.* (1990a). Residues for which internal motions contribute to T_1 or for which conformational exchange gives rise to shortened values of T_2 were identified by comparing the T_1/T_2 ratios observed for individual ^{15}N spins with the average T_1/T_2 ratio, $\langle T_1/T_2 \rangle$. When disregarding the residues for which T_1/T_2 is outside of the standard

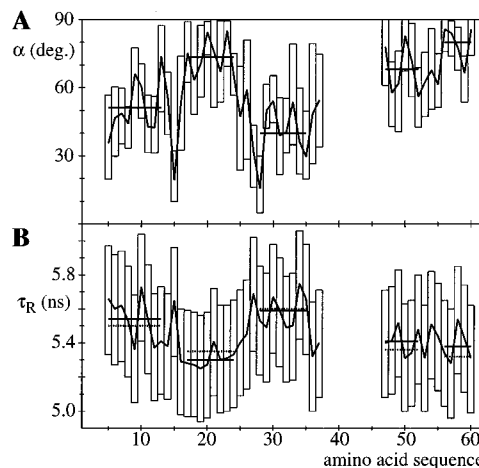


FIGURE 2: Plots of (A) the angle α between the N–H bond vector and the axis of symmetry of global molecular motion in 434(1–63) and (B) the best-fit values of the apparent spherical top correlation time, τ_R , for the individual ^{15}N nuclei versus the amino acid sequence. In panel A, the horizontal lines represent the average value of α for the individual helices. In panel B, the solid horizontal lines represent the average τ_R values for the individual helices and the broken lines the τ_R values estimated with the assumption that $\tau = 5.45$ ns and $r = 1.2$, and using the average values of α for the individual helices with the assumption that the molecular motions can be described by a rigid spherical top.

deviation, we found $\langle T_1/T_2 \rangle = 2.55 \pm 0.07$ at 400 MHz, resulting in an apparent global rotational correlation time τ_c of 5.78 ± 0.15 ns. At 750 MHz, we found that $\langle T_1/T_2 \rangle = 5.65 \pm 0.26$, affording an apparent global rotational correlation time τ_c of 5.50 ± 0.15 ns.

Global Rotational Correlation Time and Anisotropy Evaluated Using the Symmetric Top Model. The relaxation data were analyzed using the MMF by simultaneously fitting S^2 and an apparent spherical top correlation time, τ_R , for each individual ^{15}N spin. A plot of the resulting best-fit values of τ_R versus the amino acid sequence of 434(1–63) is shown in Figure 2B. For residues 2–4, 38–46, and 61–63, no data are shown since the χ^2 values indicated an unsuccessful fit because of internal mobility. The longest experimental τ_R value is 5.75 ns (Leu 34, $\alpha = 36^\circ$), the shortest τ_R value 5.25 ns (Glu 19, $\alpha = 71^\circ$), and the average 5.45 ± 0.13 ns. Following Schurr *et al.* (1994), we assume that these two residues represent α values of 0 and 90° , and thus, the resulting value for R of 1.10 corresponds to an anisotropy of the molecular tumbling of an r of ~ 1.20 (eq 10).

On the basis of the NMR solution structure of 434(1–63) at pH 4.8 (Pervushin *et al.*, 1996), the ratio of the three principal axes of inertia is 1.00:1.17:1.35. In hydrodynamic calculations using the aforementioned bead models, the ratio of the corresponding diffusion coefficients was calculated to be 1.00:1.09:1.26 for a bead radius σ of 3.5 Å at the C^α positions or 1.00:1.11:1.32 for representation of the amino acid residues by three beads with a σ of 1.0 Å at the positions of the backbone atoms N, C^α , and C' . The results of these hydrodynamic calculations thus coincide rather well with the ratios of the principal axes of inertia in the NMR structure and give a satisfactory estimate of the actually measured global rotational anisotropy.

In the symmetric top approximation, we assume that the axis of symmetry is the longest principal axis of inertia, which has the largest diffusion coefficient. On the basis of

Table 1: Correlation between the Apparent Spherical Top Correlation Times Calculated for Individual Helices of 434(1–63), τ_R , and the Angles between Backbone N–H Bond Vectors and the Axis of Symmetry of the Symmetric Top, α

residues	α (deg) ^a	τ_R experimental ^{a,b} (ns)	τ_R calculated ^c (ns)
5–13 (helix 1) ^d	51.2 ± 12.0 (35.5–73.8)	5.54 ± 0.12 (5.36–5.73)	5.50
17–24 (helix 2)	73.4 ± 7.8 (63.3–85.2)	5.30 ± 0.05 (5.25–5.41)	5.35
28–35 (helix 3)	39.9 ± 12.3 (15.5–54.2)	5.59 ± 0.09 (5.49–5.75)	5.60
47–52 (helix 4) ^e	68.1 ± 10.2 (56.1–83.0)	5.41 ± 0.07 (5.31–5.52)	5.36
56–60 (helix 5)	79.9 ± 7.4 (66.4–85.8)	5.38 ± 0.09 (5.28–5.54)	5.32

^a The numbers given are the average, $\langle\alpha\rangle$ and $\langle\tau_R\rangle$, respectively, \pm standard deviation for all residues in a given helix, with the minimum and maximum values for individual residues given in parentheses. ^b τ_R estimated from the experimental relaxation data with the assumption of a spherical top molecule undergoing fast internal motion (described by the MMF, with single-order parameter S_i^2). ^c τ_R estimated from relaxation data calculated with the assumption of a rigid spherical top molecule, using $\tau = 5.45$ ns, $r = 1.2$, and the average of the α values of the residues in the given helix. ^d Residues 2–4 were excluded because they display internal mobility. ^e Leu 45 was excluded because of internal mobility, and for Pro 46, no relaxation data are available.

the NMR solution structure of 434(1–63) at pH 4.8 (Pervushin *et al.*, 1996), the angle α between the N–H bond vector and the axis of symmetry was calculated for each residue (Figure 2A). Considering that the N–H bond vectors in an α -helix are parallel to the helix axis, with a rmsd value of about 15° (Table 1), anisotropic tumbling will cause the individual N–H moieties within a given helix to relax rather uniformly. In contrast, amide groups in different helices will generally relax at different rates, depending on the orientation of the helix axis relative to the anisotropic molecular diffusion tensor. A clear-cut correlation between the average values of α and τ_R over the individual helices, $\langle\alpha\rangle$ and $\langle\tau_R\rangle$, respectively, can indeed be seen (Figure 2). The larger the angle $\langle\alpha\rangle$, the smaller the apparent spherical top correlation time $\langle\tau_R\rangle$ (Table 1), where the short fifth helix is the only exception. Since τ_R will estimate τ correctly if α is equal to the magic angle of 54.7° (see above), we expect τ to be between 5.41 and 5.54 ns (Table 1). Values of τ_R estimated using a τ of 5.45 ns, an r of 1.2, and the average values of α for the individual helices in a calculation with a rigid spherical top are also reported in Table 1 and Figure 2. The rmsd values between the average experimental values of τ_R and these estimated values of τ_R , weighted with the helix lengths, amount to 0.044 ns.

Model-Free Analysis of Intramolecular Backbone Mobility. The experimental data could be satisfactorily fitted using the MMF approach for 45 out of the total of 60 backbone amide groups in 434(1–63). These 45 residues will be referred to as the “MMF group”. In addition, residues 9, 16, 27, 38, 43–45, 61, and 62 could be appropriately described by the SMF approach (“SMF group”), and the remaining six residues (3, 39–41, 57, and 63) required the EMF approach (“EMF group”). Leu 45 is the only residue for which we observed an increase in the ^{15}N line width as a result of conformational exchange, with a $\pi\Delta_{\text{ex}}$ of 1.0 Hz (see eq 4). Figure 3 shows the following locations of the SMF and EMF residues in the three-dimensional structure. Asn 16 and Thr

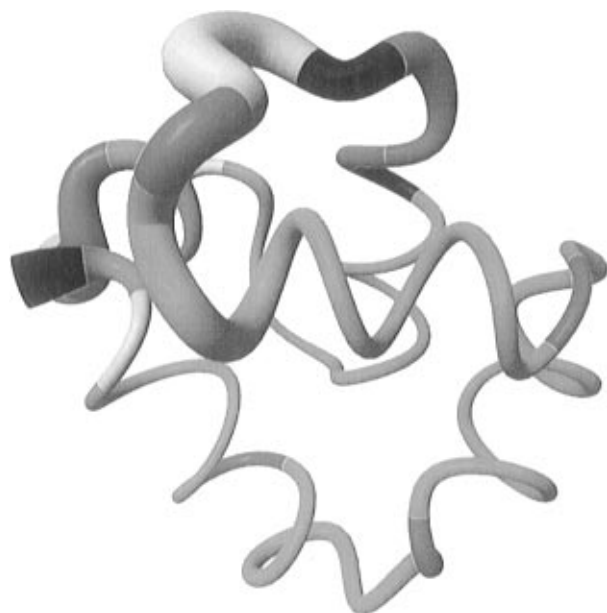


FIGURE 3: Representation of the polypeptide backbone of 434(1–63) by a spline function through the C^α positions. The variable radius of the cylinder is proportional to the average of the pairwise global backbone displacements between the 20 individual conformers used to represent the NMR structure and the average structure after superimposing the backbone atoms N, C^α , and C' of residues 2–35 and 45–60 for the best fit. The color coding is as follows: cyan, residues for which the ^{15}N relaxation data could be fitted using the minimal model-free approach (MMF group); red, residues for which the relaxation data could be fitted using the simple model-free approach (SMF group); green, Leu 45 for which the relaxation data could be fitted using the SMF plus an exchange term (eq 4); yellow, residues for which the relaxation data could only be fitted using the extended model-free approach (EMF group); and black, Ser 1, Pro 42, and Pro 46, for which ^{15}N relaxation data are not available.

27 lie in loop regions immediately preceding helix 2 and helix 3, respectively. Residues 38–45 lie in the loop between the first and second subdomain, which shows increased conformational disorder in the NMR solution structure (Pervushin *et al.*, 1996). On the basis of the relaxation data, we can now attribute the reduced precision of the structure determination for this loop to increased internal mobility. Increased local backbone mobility is similarly implicated for the C-terminal segment 61–63 and for Ser 3. Overall, Figure 3 reveals that, for the majority of residues, internal backbone dynamics inferred by the relaxation data correlates with increased conformational disorder in the NMR solution structure. Exceptions are residues 3, 9, 16, 27, 44, 45, and 57, which show local mobility but are well defined in the NMR solution structure, and residues 35–37, for which there is no indication of local mobility but which are not well defined in the NMR solution structure.

The model-free analysis was performed for both a spherical top molecule and a symmetric top molecule. For the spherical top assumption, τ_c was found to be 5.78 ± 0.15 ns at 400 MHz and 5.50 ± 0.15 ns at 750 MHz. Therefore, τ (see eq 5) was set to the average value of 5.64 ns, which lies within one standard deviation of both measured values of τ_c . In this approximation, T_1 at 400 MHz is slightly underestimated, and T_1 at 750 MHz is slightly overestimated. For the symmetric top assumption (see eqs 6–8), τ was set to 5.45 ns, $r = 1.2$, and the orientations of the N–H bond vectors with respect to the axes of rotational diffusion were evaluated from hydrodynamic calculations based on the atom

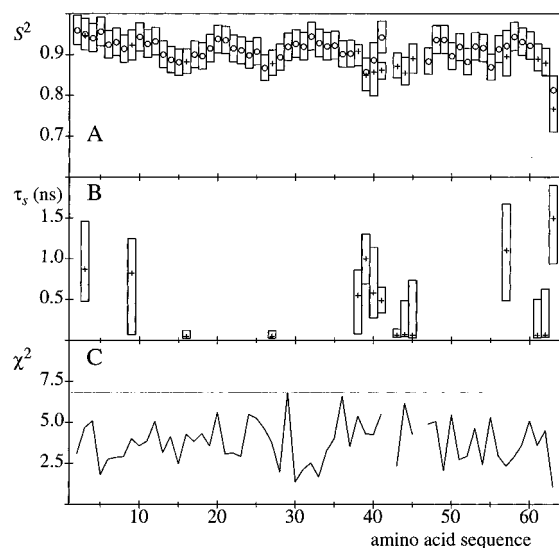


FIGURE 4: Plots of the model-free parameters determined to describe the internal backbone dynamics of 434(1–63) with the assumption that the global molecular motions can be described by a spherical top with a τ of 5.64 ns versus the amino acid sequence. (A) Generalized order parameter, where S^2 values are represented by circles (O) and S_s^2 values by plus signs (+). (B) Effective internal correlation time, τ_s , for the slower internal motion. The vertical bars indicate the estimated precision of the extracted model-free parameters (see the text). (C) χ^2 values for the fits of the relaxation data by the corresponding model-free parameters. The thin line indicates the value 6.8, below which the model-free parameters were considered to provide an adequate fit of the experimental data (Nicholson *et al.*, 1995).

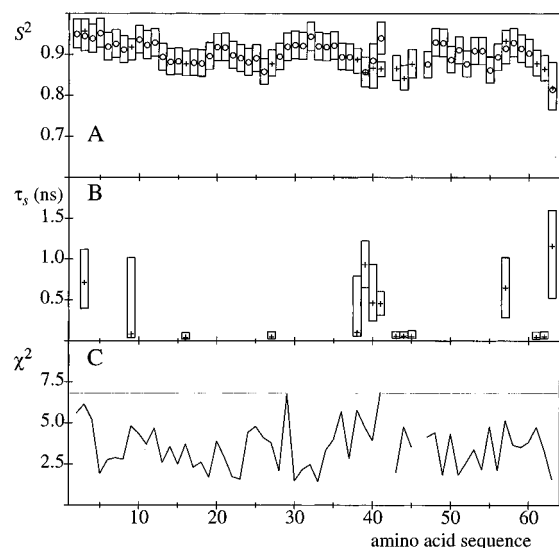


FIGURE 5: Same as Figure 4 with the assumption that the global molecular motions can be described by a symmetric top with a τ of 5.45 ns and an r of 1.2.

coordinates of the NMR structure. The resulting model-free parameters are shown in Figures 4 and 5. The values of the order parameters are very similar in both cases, with the average value of $S^2 = S^2 S_s^2$ for the helical residues equal to 0.92 ± 0.02 for the spherical top assumption and 0.91 ± 0.02 for the symmetric top assumption. Figure 6 shows that small values of the order parameter S^2 correlate with increased global backbone displacements of the NMR structure (Pervushin *et al.*, 1996) throughout the 434(1–63) molecule. Table 2 gives a summary of the model-free parameters for those residues which were found to display slow internal motions ($\tau_s > 0.5$ ns) when using the spherical

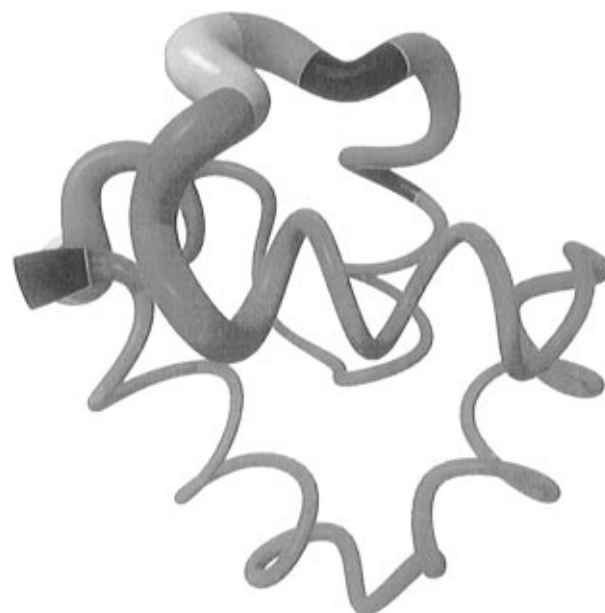


FIGURE 6: Same presentation of the polypeptide backbone of 434(1–63) as in Figure 3. The cylinder is color coded to display the continuous variation of the order parameter S^2 for the individual residues, with blue for $S^2 = 1$ through red for $S^2 = 0.85$ to yellow for $S^2 = 0.70$. Ser 1, Pro 42, and Pro 46, for which ^{15}N relaxation data are not available, are black.

Table 2: Comparison of the Model-Free Parameters Obtained Assuming either Isotropic or Anisotropic Global Rotational Diffusion for Those Residues in 434(1–63) for Which the Isotropic Model Implicated Slow Internal Motions

residue	group ^a	isotropic model ^b			anisotropic model ^c		
		S^2 ^d	τ_s (ns)	χ^2 ^e	S^2 ^d	τ_s (ns)	χ^2 ^e
Ser 3	EMF	0.90	0.87	4.7	0.90	0.71	6.1
Lys 9	SMF	0.92	0.88	4.0	0.92	0.08	4.8
Lys 38	SMF	0.91	0.55	5.4	0.89	0.10	5.8
Thr 39	EMF	0.73	1.00	4.3	0.73	0.93	4.7
Lys 40	EMF	0.76	0.58	4.2	0.77	0.46	3.9
Asp 57	EMF	0.82	1.10	2.3	0.85	0.65	5.1
Thr 63	EMF	0.62	1.49	1.0	0.67	1.16	1.6

^a SMF denotes a residue for which the experimental relaxation data could be appropriately described by the simple model-free approach. EMF denotes a residue for which the relaxation data could be satisfactorily analyzed only with the extended model-free approach. ^b The effective correlation time for isotropic global rotational reorientation $\tau = 5.64$ ns (see the text). ^c The effective correlation time for anisotropic global rotational reorientation $\tau = 5.45$ ns, and the anisotropy $r = 1.2$ (see the text). ^d $S^2 = S^2 S_s^2$. ^e The penalty function χ^2 was calculated according to eq 16. The fit of the experimental data for an individual residue is considered to be adequate for χ^2 values smaller than 6.8 (Nicholson *et al.*, 1995).

top assumption and compares these data with the corresponding model-free parameters obtained using the symmetric top assumption. In all cases, the use of the anisotropic global rotational model leads to shorter correlation times for the implicated local intramolecular motions. This effect is particularly pronounced for the two residues in the SMF group which show slow internal motions in the isotropic model (Lys 9 and Lys 38).

DISCUSSION

There were two principal reasons for choosing 434(1–63) for the present study. (i) This protein is highly soluble in water and is sufficiently small to provide excellent NMR spectral resolution. High-quality measurements of spin

relaxation parameters at different field strengths could thus be obtained. (ii) The molecular shape shows only small anisotropy. Detailed analysis of high-quality spin relaxation parameters could thus be expected to reveal how critical it is to account even for only slightly anisotropic global rotational motions in model-free approaches to characterization of the molecular dynamics. If anisotropy of the rotational tumbling should turn out to be important for 434(1–63), one would have a strong indication that much care needs to be used very generally when applying the assumption of isotropic rotational tumbling to the analysis of spin relaxation data in proteins.

A fundamental assumption inherent in the model-free approach is that the intramolecular motions must relax rapidly compared to the global rotational tumbling of the molecules, since otherwise the “decorrelation approximation” and the associated factorization of the correlation function into contributions from global and local motions may no longer be valid. As a rule of thumb, the correlation times for the internal motions should be at least 1 order of magnitude shorter than those for the global motions (Lipari & Szabo, 1982a,b). Experience has shown that the EMF may implicate slow internal motions on the nanosecond time scale (Clore *et al.*, 1990b) so that the local internal motion and the global motions would be on similar time scales. One can then not exclude the possibility that the different types of motions are correlated and that one is therefore outside of the range of validity of the model-free approach. Schurr *et al.* (1994) demonstrated with theoretical model calculations that the model-free approach can compensate for anisotropic global rotational diffusion by ascribing to most of the nuclei fictitious slow internal motions with correlation times in the nanosecond time range. Although this does not mean that such motions cannot be present in proteins, these simulations indicate that, as a compensation for the fact that the global rotational motions are actually anisotropic, slow internal dynamics can be artifactually implicated by a model-free analysis of relaxation data that assumes isotropic global rotational motions.

In 434(1–63), residues Ser 3, Lys 9, Lys 38, Thr 39, Lys 40, Asp 57, and Thr 63 violate the aforementioned decorrelation condition in the isotropic model if the relaxation data of residues 9 and 38 are interpreted by the SMF and those of residues 3, 39, 40, 57, and 63 by the EMF (Table 2). In a similar analysis that allows for anisotropic global rotation, the two residues in the SMF group exhibit significantly shorter internal correlation times (Table 2), which implies that it was the assumption of a spherical top molecule that led to artifactually long internal correlation times. Since the apparent anisotropy amounts to only 1.2, the 5–10-fold overestimate of the internal correlation times τ_s is rather impressive. Shorter internal correlation times with the use of a symmetrical top are also obtained for the residues in the EMF group (Table 2), but with the exception of residue 40, the decorrelation approximation remains violated so that the spherical top approximation seems not to account entirely for the long internal correlation times. A plausible explanation is that these residues actually display internal motions on a time scale close to that for the global rotations but that the model-free approach cannot be used for quantitative evaluation of their correlation times and order parameters because of possible correlation of the internal motions with the overall rotational tumbling. This also supports the

intuitive physical picture in which the motions of mobile loops or the chain-terminal polypeptide segments on the surface of small proteins correlate with the global rotational tumbling. Direct evidence in 434(1–63) that the spherical top approximation causes systematic deviations in the estimation of the correlation times for internal motions comes from the observation that the apparent spherical top correlation times, τ_R , determined for the groups of ^{15}N spins in the individual helices correlate with the orientation of the helix axis relative to the longest principal axis for anisotropic global rotational diffusion.

A recent publication on the analysis of relaxation data in an HIV protease (Tjandra *et al.*, 1996) reports results that are in nice agreement with and complement the present data on 434(1–63). The rotational diffusion tensor was evaluated from the relations between the T_1/T_2 ratios of individual backbone amide groups at two magnetic field strengths and their N–H orientation in the three-dimensional protein structure. The resulting diffusion tensor is nearly colinear with the tensor of inertia, and the relative magnitudes of its principal axes are in good agreement with hydrodynamic modeling results. It was further found that the lack of consideration of the anisotropy of the global rotational diffusion had little influence on the order parameters but that it caused erroneous identification of exchange broadening for four residues which have the N–H bond oriented nearly parallel (within 30°) to the molecular axis with the largest diffusion coefficient (Nicholson *et al.*, 1995).

We have also placed the experimental data on 434(1–63) in context with model considerations on the effects of larger molecular anisotropies. For this, $T_1(^{15}\text{N})$, $T_2(^{15}\text{N})$, and $^{15}\text{N}\{-^1\text{H}\}$ -NOEs were calculated for a hypothetical symmetric top molecule with an anisotropy r of 2.0 and an average global correlation time τ of 5.45 ns (see eq 8), considering different values of the angle α between the N–H bond vector and the axis of symmetry. Only rapid internal motions were considered, with an S_s^2 of 0.80 and a τ_s of 0.05 ns. The simulated relaxation data were subjected to model-free analysis with the assumption of a spherical top molecule, and the resulting best-fit model-free parameters were compared with the actual values of the parameters describing the internal motions. (i) When $0^\circ \leq \alpha \leq 36^\circ$, the simulated data could not be fitted appropriately with either the SMF or the EMF approach. If, however, an exchange term (see eq 4) was used in the SMF approach, the data could be fitted, with an S_s^2 of 0.64–0.72, a τ_s of 0.03 ns, and a $\pi\Delta_{\text{ex}}$ of 1.8–3.6 Hz. S_s^2 and τ_s were thus significantly underestimated, and the assumption of a spherical top molecule caused the erroneous identification of exchange broadening. (ii) When $37^\circ \leq \alpha \leq 90^\circ$, the simulated relaxation data could be fitted adequately with the assumption of a spherical top molecule when using either the SMF or the EMF approach. The SMF approach only slightly overestimated the actual values for S_s^2 and τ_s , with an S_s^2 of 0.80–0.82 and a τ_s of 0.05–0.06 ns, but the corresponding fit of the simulated NMR relaxation data was not acceptable. When $37^\circ \leq \alpha \leq 59^\circ$, the EMF approach yielded an S^2 of 0.81–0.82 and a τ_s of 0.05–0.11 ns, and when $60^\circ \leq \alpha \leq 90^\circ$, the EMF parameters were an S^2 of 0.73–0.80 and a τ_s of 0.26–0.81 ns. Although the best-fit S^2 values in the EMF analysis remained quite close to the actual values, the best-fit τ_s values overestimated the actual data by up to a factor 2 for the range $37^\circ \leq \alpha \leq 59^\circ$ and by a factor of 5–16 for the range $60^\circ \leq$

$\alpha \leq 90^\circ$. Overall, due to the larger number of adjustable parameters, when compared to SMF, the EMF treatment yielded an improved fit of the relaxation data, but it provided a misleading view of the internal motions. The results of these theoretical model calculations coincide closely with previous theoretical investigations of the effects of anisotropic global rotational diffusion on the performance of the SMF and EMF approaches reported by Schurr *et al.* (1994).

ACKNOWLEDGMENT

We thank Dr. F. Damberger for helpful discussions and Mrs. R. Hug for the careful processing of the manuscript.

REFERENCES

- Abragam, A. (1961) *Principles of Nuclear Magnetism*, Clarendon Press, Oxford.
- Allerhand, A., Chen, F., & Gutowsky, H. S. (1965) *J. Chem. Phys.* 42, 3040–3047.
- Barbato, G., Ikura, M., Kay, L. E., Pastor, R. W., & Bax, A. (1992) *Biochemistry* 31, 5269–5278.
- Bartels, C., Xia, T., Billeter, M., Güntert, P., & Wüthrich, K. (1995) *J. Biomol. NMR* 5, 1–10.
- Brennan, R. G., & Matthews, B. W. (1989) *J. Biol. Chem.* 264, 1903–1906.
- Broadhurst, R. W., Hardman, C. H., Thomas, J. O., & Laue, E. D. (1995) *Biochemistry* 34, 16608–16617.
- Clare, G. M., Driscoll, P. C., Wingfield, P. T., & Gronenborn, A. M. (1990a) *Biochemistry* 29, 7387–7401.
- Clare, G. M., Szabo, A., Bax, A., Kay, L. E., Driscoll, P. C., & Gronenborn, A. M. (1990b) *J. Am. Chem. Soc.* 112, 4989–4991.
- Dötsch, V., Wider, G., Siegal, G., & Wüthrich, K. (1995) *FEBS Lett.* 366, 6–10.
- Farrow, N. A., Muhandiram, R., Singer, A. U., Pascal, S. M., Kay, C. M., Gish, G., Shoelson, S. E., Pawson, T., Forman-Kay, J. D., & Kay, L. E. (1994a) *Biochemistry* 33, 5984–6003.
- Farrow, N. A., Zhang, O., Forman-Kay, J. D., & Kay, L. E. (1994b) *J. Biomol. NMR* 4, 727–734.
- García de la Torre, J., & Bloomfield, V. A. (1981) *Q. Rev. Biophys.* 14, 81–139.
- Güntert, P., Dötsch, V., Wider, G., & Wüthrich, K. (1992) *J. Biomol. NMR* 2, 619–629.
- Hiyama, Y., Niu, C., Silverton, J. V., Bavoso, A., & Torchia, D. A. (1988) *J. Am. Chem. Soc.* 110, 2378–2383.
- John, B. K., & McClung, R. E. D. (1982) *J. Magn. Reson.* 50, 267–273.
- Kamath, U., & Shriver, J. W. (1989) *J. Biol. Chem.* 264, 5586–5592.
- Kay, L. E., Torchia, D. A., & Bax, A. (1989) *Biochemistry* 28, 8972–8979.
- Kinosita, K., Kawato, S., & Ikegami, A. (1977) *Biophys. J.* 20, 289–305.
- Li, Y., & Montelione, G. T. (1994) *J. Magn. Reson. B* 105, 45–51.
- Lipari, G., & Szabo, A. (1980) *Biophys. J.* 30, 489–506.
- Lipari, G., & Szabo, A. (1982a) *J. Am. Chem. Soc.* 104, 4546–4559.
- Lipari, G., & Szabo, A. (1982b) *J. Am. Chem. Soc.* 104, 4559–4570.
- London, R. E., & Avitabile, J. (1978) *J. Am. Chem. Soc.* 100, 7159–7165.
- McConnell, H. M. (1958) *J. Chem. Phys.* 28, 430–431.
- Mondragon, A., Subbiah, S., Almo, S. C., Drott, M., & Harrison, S. C. (1989) *J. Mol. Biol.* 205, 189–201.
- Neri, D., Billeter, M., & Wüthrich, K. (1992) *J. Mol. Biol.* 223, 743–767.
- Nicholson, L. K., Yamazaki, T., Torchia, D. A., Grzesiek, S., Bax, A., Stahl, S. J., Kaufman, J. D., Wingfield, P. T., Lam, P. Y. S., Jadhav, P. K., Hodge, N., Domaille, P. J., & Chang, C. (1995) *Nat. Struct. Biol.* 2, 274–280.
- Orekhov, V. Yu., Pervushin, K. V., & Arseniev, A. S. (1994) *Eur. J. Biochem.* 219, 887–896.
- Orekhov, V. Yu., Pervushin, K. V., Korzhnev, D. M., & Arseniev, A. S. (1995a) *J. Biomol. NMR* 6, 113–122.
- Orekhov, V. Yu., Nolde, D. E., Golovanov, A. F., Korzhnev, D. M., & Arseniev, A. S. (1995b) *Appl. Magn. Reson.* 9, 581–588.
- Palmer, A. G., Rance, M., & Wright, P. E. (1991) *J. Am. Chem. Soc.* 113, 4371–4380.
- Palmer, A. G., Skelton, N. J., Chazin, W. J., Wright, P. E., & Rance, M. (1992) *Mol. Phys.* 75, 699–711.
- Peng, J., & Wagner, G. (1992) *J. Magn. Reson.* 98, 308–332.
- Peng, J., Thanabal, V., & Wagner, G. (1991) *J. Magn. Reson.* 94, 82–100.
- Pervushin, K., Billeter, M., Siegal, G., & Wüthrich, K. (1996) *J. Mol. Biol.* 264, 1002–1012.
- Press, W. H., Teukolsky, S. A., Vetterling, W. T., & Flannery, B. P. (1992) *Numerical Recipes in Fortran: The Art of Scientific Computing*, 2nd ed., Cambridge University Press, Cambridge.
- Richarz, R., Nagayama, K., & Wüthrich, K. (1980) *Biochemistry* 19, 5189–5196.
- Schurr, J. M., Babcock, H. P., & Fujimoto, B. S. (1994) *J. Magn. Reson. B* 105, 211–224.
- Shimizu, H. (1962) *J. Chem. Phys.* 37, 765–778.
- Szyperski, T., Luginbühl, P., Otting, G., Güntert, P., & Wüthrich, K. (1993) *J. Biomol. NMR* 3, 151–164.
- Tjandra, N., Kuboniwa, H., Ren, H., & Bax, A. (1995) *Eur. J. Biochem.* 230, 1014–1024.
- Tjandra, N., Wingfield, P., Stahl, S., & Bax, A. (1996) *J. Biomol. NMR* 8, 273–284.
- Tropp, J. (1980) *J. Chem. Phys.* 72, 6035–6043.
- Wagner, G. (1993) *Curr. Opin. Struct. Biol.* 3, 748–754.
- Wallach, D. (1967) *J. Chem. Phys.* 47, 5258–5268.
- Wittebort, R. J., & Szabo, A. (1978) *J. Chem. Phys.* 69, 1722–1736.
- Woessner, D. (1962a) *J. Chem. Phys.* 36, 1–4.
- Woessner, D. (1962b) *J. Chem. Phys.* 37, 647–654.
- Woessner, D. (1965) *J. Chem. Phys.* 42, 1855–1859.

BI963161H